

Mixed Convection in a Ventilated Concentric Horizontal Cylindrical Annulus for Aiding and Opposing Buoyancy Forces

Latifa Begum^{1*}, Tonny Tabassum¹, Mainul Hasan¹

¹Department of Mining & Materials Engineering, McGill University, Canada.

*email: Latifa.begum@mail.mcgill.ca

Abstract

A numerical study of laminar mixed convective heat transfer of water in the vented annular region between the two concentric horizontal cylinders has been carried out. The diameter ratio of the outer and inner cylinders is 2.6. The forced flow conditions are imposed through the inlet opening ($\theta_{inlet}=30^\circ$) at the top of the outer cylinder around the upper symmetry plane. The smaller outlet vent ($\theta_{outlet}=10^\circ$) compared to the inlet vent is at the bottom and is placed diametrically opposite from the inlet. The inner cylinder wall is considered at a constant temperature while the outer one is insulated except the inlet and outlet ports. This geometry is suitable as a heat exchanger for solar energy applications. The two-dimensional conservative form of continuity, Navier-Stokes and the energy equations are solved by using control volume based finite difference technique on a uniform staggered grid arrangement. The Boussinesq approximation is employed to implement the natural convection terms in the momentum equations. The effect of main non-dimensional parameters governing the problem such as the Richardson number (RI) varying from $0 \leq RI \leq 2.0$ and the Reynolds number (Re_D) varying from $50 \leq Re_D \leq 200$ is considered. The nature and the basic characteristics of the aiding as well as opposing flows are numerically investigated. In the cases studied, the aiding flow is found to have a significant effect in the enhancement of average Nusselt number on the inner cylinder compared to the opposing flow. It has been also found that the average Nusselt number increases with the increase of the Reynolds number. Furthermore, it is predicted that after a certain value of the Richardson number the average Nusselt number remains practically unchanged for the both imposed flow conditions irrespective of the Reynolds number due to the insignificant effect of the buoyancy force. To get a visual understanding of the mixed convection phenomena in the vented annulus, streamlines and isotherms for various cases are also presented. Empirical correlations are developed for the average Nusselt number as a function of Richardson number and Reynolds number for the both aiding and opposing flow situations in the studied ranges.

Keywords: Laminar Mixed Convection, Numerical Study, Aiding and Opposing Flow, Vented Cavity, and Horizontal Concentric Cylinders.

NOMENCLATURE

a_p	coefficient in the discretized governing equation
D_e, D_w, D_n, D_s	diffusive conductance
F_e, F_w, F_n, F_s	strength of convection
g	gravitational acceleration, $m.s^{-2}$
h	convective heat transfer coefficient
K_{eq}	Local equivalent thermal conductivity = $\frac{Nu_L}{Nu_0}$
\bar{K}_{eq}	Circumferential average equivalent thermal conductivity = $\frac{\bar{Nu}}{Nu_0}$
L	Gap width of the annulus = $(r_o - r_i)$, m
Nu_0	Nusselt number for conduction between the annuli
Nu_L	Local Nusselt number
\bar{Nu}_{avg}	Circumferential average Nusselt number based on cylinder radius
P	Pressure, Pa
Pr	Prandtl number = $\frac{\nu_f}{\alpha_f}$
r_i	Radius of inner cylinder, m
r_o	Radius of outer cylinder, m
R_i	Dimensionless radius of inner cylinder
R_o	Dimensionless radius of outer cylinder

Ra	Rayleigh number = $\frac{g\beta_f(T_i - T_o)r_i^3\rho}{\mu\alpha_f}$
RI	Richardson number = $\frac{Gr}{Re^2} = \frac{r_i^2\beta_f g (T_o - T_i) }{v^2 Re^2}$
Re _o	Reynold number = $\frac{r_i \rho v_{in}}{\mu}$
T	Temperature, K
T _o	Temperature on cold wall, K
T _i	Temperature on hot wall, K
T _{ref}	Reference temperature (T _o), K
ϕ (for aiding flow)	Dimensionless temperature = $\frac{T - T_{ref}}{T_o - T_i}$
ϕ (for opposing flow)	Dimensionless temperature = $\frac{T - T_{ref}}{T_i - T_o}$
ϕ _i	Dimensionless temperature for inner cylinder wall = 0 K
Pc	Peclet number
Φ	Transported scalar
u, v	Interstitial velocity components along θ and r directions respectively, ms ⁻¹
U, V	Dimensionless interstitial velocity components along θ and r directions respectively
θ, r	Polar coordinates, degree and m

Greek symbols

α _f	Thermal diffusivity, m ² s ⁻¹
β _f	Coefficient of thermal expansion, $\frac{1}{T}$, K ⁻¹
ν _f	Kinematic viscosity, m ² s ⁻¹
ρ	Density, kg.m ⁻³
μ	Dynamic viscosity, kg.m ⁻¹ .s ⁻¹

Subscripts

e, w, n, s	Four surfaces of control volume centred at P
nb	Neighbouring points in numerical molecule
P	Nodal point to be solved in difference equation
i	Inner cylinder
o	Outer cylinder
ref	Reference value

1.0 INTRODUCTION

For many practical applications, the analysis of mixed convection flow and heat transfer problems in annuli is important. Mixed convection plays an important role in heat exchangers, electronic boards, combustors, thermal design of buildings, solar collectors, drilling operations, commercial refrigeration, geothermal power generation, float glass production, etc. The mixed convection is a combination of free and forced convection. In mixed convection, the free convection can either assist or oppose the forced convection which will depend on the direction of the forced convection flow and the heat transfer within the fluid. The forced convection component in the mixed convection flow is generated by the mechanical devices like a fan, a pump, rotating surfaces, etc. The free convection is generated due to the density gradient within the fluid and appears as buoyancy force. The relative magnitude of forced and free convection ultimately determines the overall flow and heat transfer patterns within the domain. In reality, the buoyancy force can be developed both due to the thermal gradient and concentration gradient. The latter two forces can either assist or oppose one another which will depend on the direction and magnitude of the thermal and concentration buoyancy forces. Moreover, mixed convection flow can be broadly characterized as externally mixed convection and internally mixed convection. Many studies exist in the literature, which has dealt with the above two mentioned categories. The present study is concerned with the internally mixed convection where only thermal buoyancy has been considered. There have been a lot of investigations published in the literature on mixed convective flow in the cavities with many different configurations and combinations of thermal boundary conditions and with various working fluids. The present study deals with a unique mixed convection problem in a concentric and partially ventilated horizontal cylindrical annulus. Since, a detailed literature search has not revealed a single study on the

above-stated problem, hence a very limited literature review is provided below to assist the readers to understand the extent of the work that has been carried out so far in this field.

In 2013, an excellent review paper was published on mixed convection flow and heat transfer in horizontal, vertical and rotating cylinders subjected to different boundary conditions as well as cylinders embedded inside a channel, annulus, and cavity by Hussein [1]. The latter author has reviewed about one-hundred published papers which were collected from different local and international journals and conferences. This review has covered the research in this field up to the year 2012. All numerical, analytical and experimental works related to mixed convection were categorically described. Obviously, this comprehensive paper can give a good overview and a solid background to future researchers and readers who are interested and will be working in the field of the combined free and forced convection flows in and around cylinders. Although in the next six years a number of papers on mixed convection in enclosed cavities have appeared in the journals and conferences, unfortunately, all the latter works are mere perturbations of the earlier studies. Below two papers are reviewed which bear some similarity with the present study.

El-Maghlany et al. [2] numerically simulated the two-dimensional double-diffusive mixed convection within a horizontal rotating annulus using the finite volume technique at steady state. The inner cylinder was allowed to rotate both clockwise and counter-clockwise directions while the outer cylinder was kept stationary. The thermal Grashof number, Prandtl number, buoyancy ratio, and the radius ratio were kept at fixed values equal to 10^4 , 0.7, 1 and 2, respectively. The two main parameters which were varied are Richardson number (Ri) and Lewis number (Le) in the range of $0.01 \leq Ri \leq 100$ and $0.01 \leq Le \leq 100$, respectively. As Ri increases the points of the minimum and maximum local Nusselt and Sherwood numbers were found to lie in the opposite direction of the inner cylinder rotation. With the increase of the Lewis number, the mass transfer is increased but no enhancement for the heat transfer has happened. With the decrease of Ri , the clockwise rotation of the inner cylinder is seen to give better heat and mass transfer compared to the anti-clockwise direction.

Recently, Jafari et al. [3] numerically investigated the steady-state 2-D laminar mixed convection flow between two horizontal cylinders using the Lattice Boltzmann method. Different eccentricities of the inner cylinder were considered while keeping the radius ratio of the outer to the inner cylinder as 2.5. Three Richardson numbers (Ri) were considered, namely 0.01, 1, 100 for air ($Pr = 0.716$) and water ($Pr = 6.2$). For the mixed convection situation, the inner cylinder was allowed to rotate whereas the outer cylinder was stationary. The most important outcome of the simulated results is that the mean Nusselt number was found to depend on the value of the Ri and the maximum value of the Nusselt number is obtained for the case of eccentric cylinders with an eccentricity of -0.75 , and $Ri = 100$ for water.

Based on the above literature review, no study seems to be there in the literature which compares the performances of imposed forced flow in a horizontal annulus where the inner cylinder is at a different temperature with respect to the temperature of the imposed fluid. The major objective of the present work is thus to study numerically the effect of mixed convection on heat transfer and flow within the annulus formed by two horizontal, concentric cylinders under both aiding and opposing buoyancy forces. This study concentrates on the characteristics of both aiding and opposing buoyant flows arising from hot/cold jets impinging from the top of the outer cylinder of the annulus and discharging through the bottom of the outer cylinder. The wall of the inner cylinder is maintained isothermal either at a temperature higher or lower than the temperature of the incoming jet of fluid. The above arrangements thus give rise to the aiding and opposing buoyancy forces with regard to the forced flow situations. The outgoing flow is assumed to be hydrodynamically and thermally fully developed. The rest of the outer (except the inlet and outlet ports) wall of the outer cylinder is insulated. To the best of authors' knowledge, no experimental or modeling work for this flow situation in the horizontal concentric cylindrical annulus is reported in the literature. Because of the unavailability of similar studies, the presented results could not be directly compared with any experimental or numerical results from the literature.

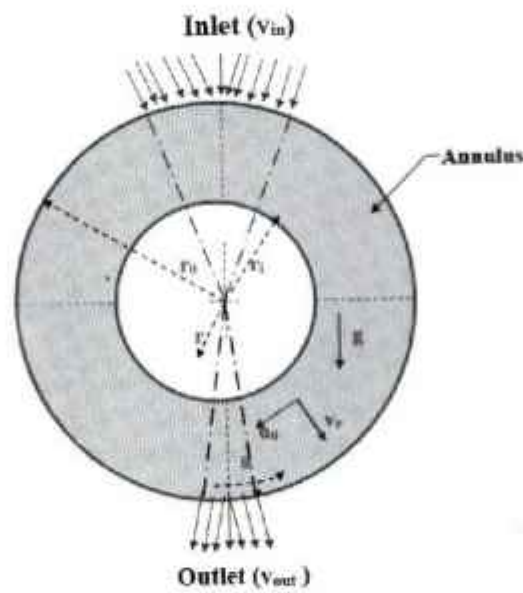


Fig. 1: Schematic diagram of a concentric and partially ventilated horizontal cylindrical annulus with coordinate system

2.0 DESCRIPTION OF THE PROBLEM

The physical model of the problem is illustrated schematically in Fig. 1. The radius of the inner cylinder is denoted by r_i while that of the outer cylinder is denoted by r_o . The inner and outer cylinders are considered to be of aluminum and their wall thickness is equal to one grid size. The inner cylinder is maintained at a uniform temperature of T_i . The cylinders are assumed to be long enough that a two dimensional analysis can be applied. The fluid under consideration is water. Due to symmetry, the computations are carried for only half of the physical domain by making use of the vertical symmetry plane passing through the center of the cylinder. The ratio of the outer radius to the inner radius is assigned a value of 2.6, which is reported in the literature to be the best geometry for obtaining the maximum heat transfer rate. It is seen from the literature [4] that a lower radius ratio leads to multiple solutions and for a greater radius ratio of more than 2.6 the importance of the outer cylinder is diminished so far the natural convection heat transfer is concerned.

3.0 MATHEMATICAL FORMULATION OF LAMINAR FLUID FLOW AND HEAT TRANSFER INSIDE THE ANNULUS

Natural convective motion is generated by the Buoyancy in between annulus in the (r, θ) plane with radial and angular velocity components. The steady-state, two-dimensionless conservation equations of mass, momentum and energy for a Newtonian fluid in conservative form under laminar mixed convection situation over a cylinder, including the Boussinesq approximation, are given as follows:

Using the Boussinesq approximation, the density term is given by

$$\rho = \rho_{ref} [1 - \beta(T - T_{ref})] \tag{1}$$

Continuity:

$$\frac{1}{R} \frac{\partial(RV)}{\partial R} + \frac{1}{R} \frac{\partial U}{\partial \theta} = 0 \tag{2}$$

U-momentum equation:

$$\frac{1}{R} \frac{\partial}{\partial R} (RUU) + \frac{1}{R} \frac{\partial}{\partial \theta} (UV) = \frac{1}{Re \times R} \frac{\partial}{\partial R} \left(R \frac{\partial U}{\partial R} \right) + \frac{1}{Re \times R} \frac{\partial}{\partial \theta} \left(\frac{1}{R} \frac{\partial U}{\partial \theta} \right) - \frac{1}{R} \frac{\partial P^*}{\partial \theta} + 2 \frac{1}{Re \times R^2} \frac{\partial V}{\partial \theta} - \frac{U}{Re \times R^2} - \frac{UV}{R} + RI \times \phi \sin \theta \quad (3)$$

V-momentum equation:

$$\frac{1}{R} \frac{\partial}{\partial R} (RUV) + \frac{1}{R} \frac{\partial}{\partial \theta} (VV) = \frac{1}{Re \times R} \frac{\partial}{\partial R} \left(R \frac{\partial V}{\partial R} \right) + \frac{1}{Re \times R} \frac{\partial}{\partial \theta} \left(\frac{1}{R} \frac{\partial V}{\partial \theta} \right) - \frac{\partial P^*}{\partial R} - 2 \frac{1}{Re \times R^2} \frac{\partial U}{\partial \theta} - \frac{V}{Re \times R^2} - \frac{U^2}{R} - RI \times \phi \cos \theta \quad (4)$$

Energy equation:

$$\frac{1}{R^2} \frac{\partial}{\partial R} (RV\phi) + \frac{1}{R} \frac{\partial}{\partial \theta} (U\phi) = \frac{1}{Pr \times Re} \frac{1}{R} \frac{\partial}{\partial R} \left(R \frac{\partial \phi}{\partial R} \right) + \frac{1}{Pr \times Re} \frac{1}{R} \frac{\partial}{\partial \theta} \left(\frac{1}{R} \frac{\partial \phi}{\partial \theta} \right) \quad (5)$$

The dimensionless variables (capitalized letters) are defined as:

$$R = \frac{r}{r_i}; \quad U = \frac{u}{v_{in}}; \quad V = \frac{v}{v_{in}}; \quad \phi (\text{for opposin } g \text{ flow}) = \frac{T - T_{ref}}{T_i - T_o}; \quad \phi (\text{for aiding flow}) = \frac{T - T_{ref}}{T_o - T_i};$$

$$RI = \frac{Gr}{Re^2} = \frac{r_i^3 \beta g (T_i - T_o)}{v^2 \times Re^2}; \quad Re = \frac{r_i \rho v_{in}}{\mu};$$

$$P^* = \frac{\rho (r_i Pr)^3}{\mu^2} \left[P + \left(\rho_{ref} (1 - \beta T_{ref}) - \frac{Pr^2 \rho^3 \beta T_{ref}}{\mu} \right) g r \cos \theta \right] \quad (6)$$

3.1 Assumptions

To realistically model the stated problem some standard assumptions have been considered. These are:

- [1]. The thickness of the inner and outer cylinders coincides with one grid spacing.
- [2]. The flow of the working fluid (water) is steady, laminar, and independent of the axial direction.
- [3]. No-slip conditions are applicable for the velocity components at the solid boundaries.
- [4]. The angular gradients of the temperature, radial velocity, and angular velocity are all zero at the axis of symmetry.

The thermo-physical properties of the fluid are temperature-independent, except for the density, for which the Boussinesq approximation is applicable. Viscous dissipation, compressibility effects and radiation are neglected.

3.2 Boundary Conditions

The right-half of the annulus is chosen as the solution domain as shown in Fig. 1. The dimensionless boundary conditions corresponding to this problem are presented as follows:

- [1]. On the inner cylinder surface, i.e., $R_i = 1.0$; $U = V = 0$; $\phi_i = 0$
- [2]. On the outer cylinder surface except inlet and outlet ports, i.e., $R_o = 2.6$; $U = V = 0$; $\frac{\partial \phi}{\partial R} = 0$
- [3]. Lower plane of symmetry; i.e., $\theta = 0$; $U = 0$; $\frac{\partial V}{\partial \theta} = \frac{\partial \phi}{\partial \theta} = 0$.
- [4]. Upper plane of symmetry; i.e., $\theta = \pi$; $U = 0$; $\frac{\partial V}{\partial \theta} = \frac{\partial \phi}{\partial \theta} = 0$

- [5]. At the inlet port ($R_0=2.6, \theta = 165^\circ$ to π); i.e., $U = 0; V = 1.0, \phi_{inlet} = 1.0$ for the adding flow and $U = 0; V = 1.0, \phi_{inlet} = -1.0$ for the opposing flow.
- [6]. At the outlet port ($R_0=2.6, \theta = 0^\circ$ to 5°); i.e., $U = 0; \frac{\partial \phi}{\partial R} = \frac{\partial V}{\partial R} = 0$

3.3 Numerical Solution Procedure

The first step in numerical solution is to provide the algebraic form of transport equations at appropriately chosen grid points. This operation is termed ‘discretization’. Discretization equations are derived by integration of the partial differential equations over each control volume of the domain. To solve the discretized transformed governing equations, a program based on the control volume finite difference (CVFD) was written. Patankar’s SIMPLER algorithm [5] was used to resolve the pressure-velocity coupling in the momentum equations. The general form of the algebraic governing equations obtained from the discretization can be written in the following general form:

$$a_p \Phi_p = a_E \Phi_E + a_w \Phi_w + a_N \Phi_N + a_S \Phi_S + b_\Phi \tag{7}$$

Here, a_E, a_w, a_N, a_S are the coefficients of the neighboring nodes and b_Φ is the source term corresponding to the variable Φ . With this computational procedure the whole domain is described by a displaced or staggered grid system as shown in Fig. 2. The scalar quantities (P, T) are located at the middle of the scalar control volume shown by the farm line (green color), while the velocity components (U and V) are located at the faces of the scalar control volumes and their control volumes are presented by dotted lines (blue and pink colors). The advantages of the staggered grid are twofold: firstly, the mass flow rates across the control volume faces can be calculated without any interpolation from adjacent velocities and secondly, the pressure difference between two adjacent grid points becomes the natural driving forces for the velocity components located between these grid points.

The variable U denotes the velocity in the θ -direction at the ‘e’ and ‘w’ locations of the east and west faces. Similarly, the variable V denotes the velocity in the r-direction at the ‘n’ and ‘s’ locations of the north and south faces. Integration of convective diffusion equations over the control volume involves approximating the value of Φ at the control volume surfaces. The approximation can be done using different schemes. Here power-law scheme [5] was used to discretize the convective derivatives in the main flow direction.

The generalized formula for the neighbor point coefficients for each schemes are as follows:

$$a_E = D_e A(Pe_e) + \max(F_e, 0)$$

$$a_w = D_w A(Pe_w) + \max(F_w, 0)$$

$$a_N = D_n A(Pe_n) + \max(F_n, 0)$$

$$a_S = D_s A(Pe_s) + \max(F_s, 0)$$

Here, D_e is diffusion conductance at interface e between P and E, and D_w, D_n and D_s are similar values in w, n, and s interfaces, respectively. F_e denotes the strength of convection at interface e between P and E and F_w, F_n and F_s are similar values in w, n, and s interfaces, respectively. Pe is Peclet number defined by the ratio of strength of convection to diffusion conductance. The operator $\max(a, b)$ is equivalent to $AMAX(A,B)$ in FORTRAN. For power-law difference scheme the formula for the function $A(Pe_e)$ is given in [5]. The general form of linearized source term is: $S_\Phi = S_C + S_P \Phi_P$, where, S_C becomes the contributor to b and S_P is a contributor to a_p in the discretized equation.

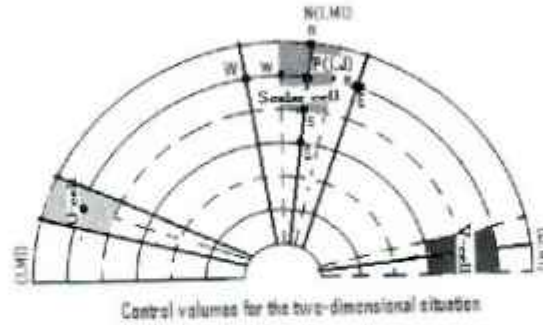


Fig. 2: Staggered grid arrangement for (r, θ) plane

3.4 Convergence Criteria

The termination of an iteration loop depends on the values of the residuals for U , V , ΔP and ϕ . The residual is defined by the general variable Φ as follows:

$$\text{Residual} = \left| \frac{\Phi^{k+1} - \Phi^k}{\Phi_{Max}^k} \right| \quad (8)$$

Where, k is the number of iteration. The convergence was achieved when the maximum absolute value of the residuals were less than 10^{-4} . A block correction procedure [5] was used to enhance the convergence of the solution procedure.

3.5 Under-Relaxation Factor

The nonlinearity and inter-linkage of the governing equations may appreciably change the results from iteration to iteration. These rapid changes influence the magnitude of the coefficients of the tri-diagonal matrix which then generally leads to divergence of the algebraic equations. To prevent the program from divergence, under-relaxation parameters were introduced for velocities and temperature. Use of the implicit form of under-relaxation before solution of the algebraic equations, changes the coefficients of these equations as follows:

$$\frac{a_p}{\alpha_\phi} \Phi_p = \sum_{nb} a_{nb} \Phi_{nb} + b_\phi + (1 - \alpha_\phi) \frac{a_p}{\alpha_\phi} \Phi_p^* \quad (9)$$

Where, α_ϕ is the under relaxation factor for the general variable Φ . The suitable values of the relaxation factor were found by experience since they depend upon a number of factors (grid resolution, Rayleigh number, Reynolds number, etc.). In the present study, much effort has been paid to find the relevant under-relaxation factors. Various combinations of under-relaxation factors were examined and after numerous runs the following under-relaxation factors were selected for the production runs: $\alpha_u = 0.3$; $\alpha_v = 0.3$; $\alpha_T = 0.4$; and $\alpha_{PC} = 0.1$.

4.0 NUMERICAL CODE VERIFICATION

The lack of experimental data for the present work forced us to carry out the code verification with the available experimental results in the literature. The accuracy of the present numerical results was investigated by computing natural convection in a concentric horizontal annular region for air. Various authors have studied this configuration in detail and established to an extent that is used as a source of comparison for validating the numerical codes. Here, the present numerical code is extensively validated against the experimental and numerical results of Kuhen and Goldstein [4] and numerical results of Hessami et al [6], Yang et al [7], Marie-Isabelle et al [8]. Table 1 presents a comparison between the present numerical results with the available experimental results of Kuhen and Goldstein [4] and numerical results of others. The values of the dimensionless parameters were chosen exactly the same as others so as to facilitate the comparison with the available experimental and numerically predicted data. An equivalent average thermal conductivity ($\overline{K_{eq}}$) on the outer surface of the inner cylinder and inner surface of the outer cylinder was used to compare the accuracy of the present computations. This parameter is defined as the ratio of actual heat flux to the heat flux that would have occurred due to pure conduction without the convective motion of the working fluid. Many authors have used the value of $\overline{K_{eq}}$ on the inner and outer cylinders as a suitable criterion for the accuracy of their numerical procedures. This choice may yield an error in computing the actual heat transfer rate since various authors

have used various expressions for calculating the conductive heat transfer rate. In this study, one dimensional conduction equation was solved to compute the heat flux without the fluid motion (defined in Eqn. 12). It can be seen in Table 1 that the present numerical results are in very good agreement with the experimental results of Kuehn and Goldstein [4] for Rayleigh number of 5×10^4 , $Pr = 0.7$ and non-dimensional diameter ratio of 2.6. The percentage of error was calculated with respect to the experimental results presented by Kuehn & Goldstein. The difference between the experimental and the present numerical results for $\overline{K_{eq_i}}$ is less than 1.5% for the inner and about 2.2% for the outer cylinder. The errors in the numerical result may arise from the constant-property assumption, the finite number of nodes, the convergence level of the solution, etc. The numerical analysis has the advantage of obtaining and observing the velocity field which is difficult to obtain experimentally. In addition, an overall energy balance was made, i.e., the integrated heat transfer rate through the inner cylinder must be equal to that of the outer cylinder. The discrepancy between the heat transfer rates was found to be less than 3.6%.

Table 1: Comparison of present results for $Pr = 0.7$ with experimental and numerical results of others

Parameter	Kuehn & Goldstein exp. [4]	Kuehn & Goldstein num. [4]	Hessami et al num. [6]	Yang et al num. [7]	Marie et al num. [8]	Present numerical computation
Ra_i	4.7×10^4	5.0×10^4	5.0×10^4	4.7×10^4	5.0×10^4	5.0×10^4
Pr	0.706	0.7	0.7	0.7	0.7	0.7
$\overline{K_{eq_i}}$ on inner cylinder	3.0	3.024	3.26	2.943	2.955	3.044
Percent of error	0.0%	0.8%	8.7%	1.9%	1.5%	1.5% over
$\overline{K_{eq_o}}$ on outer cylinder	3.0	2.973	3.05	2.901	2.955	2.935
Percent of error	0.0%	0.9%	1.7%	3.3%	1.5%	2.2% over

Figure 3 shows the comparison between the present numerically predicted data and Kuehn and Goldstein's [4] numerically predicted local equivalent thermal conductivities along the inner and outer cylinders for Pr numbers 0.7, 1.0 and 5.0; $L/D_i = 0.8$; all for a fixed Rayleigh number of 10^4 . These results were obtained using a uniform 42×42 ($r-\theta$) grid system. It is observed from Fig. 3 that a solution similar to the one presented by Kuehn and Goldstein was obtained. These authors published results of averaged equivalent thermal conductivity for the same conditions and these results are compared in Table 2. There is excellent agreement between the present results and the results from Kuehn and Goldstein; the average equivalent thermal conductivities differ by less than 5%. This small difference may be due to the lower convergence criterion used by Kuehn and Goldstein which was 10^{-3} and in the present simulation study a ten-fold lower convergence criterion (10^{-4}) was used. Besides this, Kuehn and Goldstein used an arbitrary set of non-uniform grids while in the present numerical simulation a higher density uniform grid system was used. A detailed description of code validation can be found in [9].

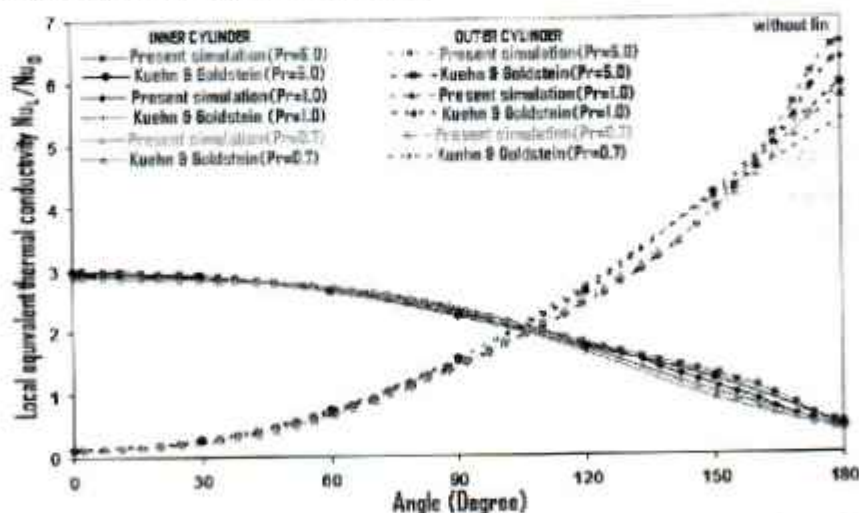


Fig. 3: Present numerical predictions versus numerically predicted data of Kuehn and Goldstein [4]

Mixed Convection in a Ventilated Concentric Horizontal Cylindrical
Annulus for Aiding and Opposing Buoyancy Forces

Table 2: Comparison between numerical results of average equivalent thermal conductivity

Parameter	Kuehn & Goldstein num. [4]	Present numerical computation	Kuehn & Goldstein num. [4]	Present numerical computation	Kuehn & Goldstein num [4]	Present numerical computation
Ra_L	10 ⁴	10 ⁴	10 ⁴	10 ⁴	10 ⁴	10 ⁴
Pr	5.0	5.0	1.0	1.0	0.7	0.7
$\overline{K_{eq_i}}$ on inner cylinder	2.069	2.119	2.038	2.089	2.010	2.05
Percent of error	0.0%	2.42%	0.0%	2.50%	0.0%	1.99%
$\overline{K_{eq_o}}$ on outer cylinder	2.066	1.994	2.039	1.951	2.005	1.933
Percent of error	0.0%	3.48%	0.0%	4.32%	0.0%	3.59%

5.0 GRID INDEPENDENT TEST

In the present work the grid distribution in the r - θ coordinates was uniform. The selection of the number of grid points used in the present computation was reasoned based on equivalent thermal conductivity prediction along the inner cylinder. To obtain grid independent results four different numbers of grid distributions were tested. The computations were carried out with 42×42 , 62×62 , 82×82 and 102×102 grid design for a Prandtl number of 1.0, annulus gap-based Rayleigh number of 10^4 and outer to inner cylinder diameter ratio of 2.6. Table 3 shows the effect

of the number of grid points on mean equivalent thermal conductivity ($\overline{K_{eq_i}}$) for the inner cylinder surface of a horizontal cylindrical annulus. As is observed from the Table 3, the difference among the mean equivalent thermal conductivity obtained for 82×82 grid points and those computed with other numbers of grid points is not very significant (an error of less than 7.0%). The effect of grid points on local equivalent thermal conductivity predictions is also investigated. Figure 4 represents the results of the local equivalent thermal conductivity variation along the inner cylinder wall for the above stated conditions. This figure shows that the local equivalent thermal conductivity prediction along the inner cylinder surface for 82×82 grid points nearly correspond to those obtained from 42×42 and 62×62 grid points, while the difference with 102×102 grid points is significant. The computations were performed on a personal computer having a speed of 2.66 GHz and fitted with a RAM of 4 Gigabytes. The number of iterations required to obtain converged solution was presented in Table 3. In view of the above results, for obtaining accurate predictions and for the sake of computational economy all production runs were performed with the 82×82 grid system which was uniform in both directions, except near the walls where non-uniformity was due to the employment of B-type staggered grids. The details of the predicted results along with the comparisons are provided in [9].

Table 3: Effect of grid points on mean equivalent thermal conductivity ($\overline{K_{eq_i}}$)

Grid points	42 × 42	62 × 62	82 × 82	102 × 102
$\overline{K_{eq_i}}$ on inner cylinder	2.1	2.14	2.18	2.33
Percent of error	3.7%	1.84%	0.0%	6.88%
No. of iterations required for the convergence	1056	1742	2701	2804

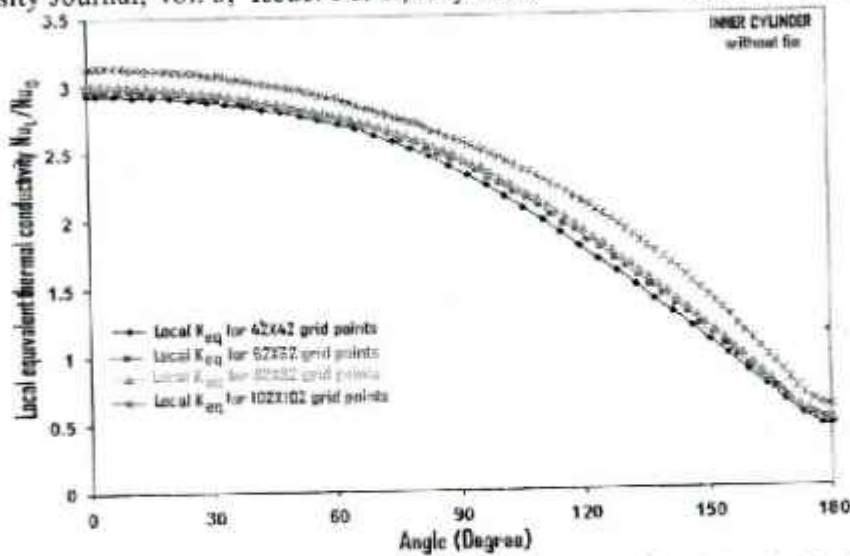


Fig. 4: Local equivalent thermal conductivity variations on the inner cylinder for Pr = 1.0, Ra = 10⁴

6.0 CHARACTERISTIC PARAMETERS

Non-dimensional Local Nusselt number along the inner cylinder is

$$Nu_{L, at R=R_i} = - \left. \frac{\partial \phi}{\partial R} \right|_{R_i=1.0} \tag{10}$$

Circumferential average Nusselt number ($\overline{Nu_{avg}}$) based on cylinder radius, which gives the net heat transfer rate through the cylinder surface, is calculated as

$$\overline{Nu_{avg}} \text{ at } r=r_i = \frac{\int_0^L \int_0^\pi (Nu_L)_{r=r_i} r_i d\theta dz}{\int_0^L \int_0^\pi r_i d\theta dz}$$

$$\overline{Nu_{avg}} \text{ at } R=R_i = - \frac{1}{\pi} \int_0^\pi \frac{\partial \phi}{\partial R} d\theta \tag{11}$$

For presenting the results two quantities are used. These are circumferential average equivalent thermal conductivity ($\overline{K_{eq_i}}$) and local equivalent thermal conductivity K_{eq} along the inner cylinder.

$$\overline{K_{eq_{inner}}} = \frac{\overline{Nu_{avg}}}{Nu_0} \text{ and } K_{eq} = \frac{Nu_L}{Nu_0}$$

Nu_0 = Nusselt number for conduction between the annuli. The subscript 0 indicates Nusselt number for conduction heat transfer in the annulus. This is obtained by solving the one-dimensional conduction equation at steady state which is given by

$$\frac{1}{r} \frac{\partial}{\partial r} \left(kr \frac{\partial T}{\partial r} \right) = 0 \tag{12}$$

The Nusselt number for conduction is evaluated as

$$Nu_0 = \frac{1}{\ln \frac{R_o}{R_i}}$$

The Lagrangian interpolation scheme is used to calculate the local Nusselt number results. This interpolation scheme is used to improve the accuracy of the calculations near the solid surfaces because of the non-uniform grid distributions near the inner cylinder wall. The non-uniformity in the grid distributions near the walls is due to the employment of B-type staggered grids. The average Nusselt number is obtained by integrating the local Nusselt number over the inner cylinder, which is numerically calculated using the Simpson-rule of numerical integration of a definite integral.

7.0 RESULTS AND DISCUSSION

Flow and temperature fields, as well as heat transfer from the heated inner cylinder wall are examined where the Richardson number, RI is varied as 0, 0.1, 0.5, 1.0 and 2.0 and the corresponding ranges of Rayleigh numbers ($Gr \times Pr$) varied from 10^3 to 10^5 , Reynolds number (Re_D) is varied as 50, 100, 150 and 200, for an inlet angle, $\theta_{inlet} = 15^\circ$, and an outlet angle, $\theta_{outlet} = 5^\circ$. The values chosen for Re , are in the laminar regime. The inlet angle (θ_{inlet}), outlet angle (θ_{outlet}), the outer to inner radius ratio (2.6) of the annulus are kept fixed for a total of 40 different runs. The working fluid is chosen as water with Prandtl number, $Pr = 6.78$. At the exit, the flow is assumed to be fully developed, allowing derivatives of the radial velocity and temperature to be set to zero. Along the solid walls of the cylinder the velocities are zero, while the non-dimensional temperature on the inner cylinder surface is zero and in the inlet port is either positive one (defined as aiding flow) or negative one (defined as opposing flow) depending upon the case modeled. The above two flow situations have been employed in this modeling work. The first one, referred to as case I hereafter, involves forcing a hot fluid through the inlet port, i.e., $\phi_{inlet} = 1.0$ for the inlet fluid and $\phi_i = 0.0$ for the inner cylinder wall. The second one, referred to as case II hereafter, involves forcing a cold fluid through the inlet port, i.e., $\phi_{inlet} = -1.0$ for the inlet fluid and $\phi_i = 0.0$ for the inner cylinder wall. In this study, the definition of ϕ is different for the above two cases. It is to be noted that converged solutions could not be obtained for higher values of Reynolds number. Thus, the upper limit of the Reynolds number for which the flow stays laminar could not be ascertained in this study. The numerical results are displayed as stream function and isotherm contours in a flooded format. Variation of the local Nusselt number around the perimeter of the inner cylinder at different Reynolds numbers is provided. The average Nusselt number on the inner cylinder wall with Richardson numbers (also called buoyancy parameter or mixed convection parameter) for different Reynolds numbers are also been reported.

7.1 Characteristics of Flow and Thermal Fields for Case I

First, the predicted streamlines and isotherms contours in the flooded format inside the annulus for four cases are presented in Figs. 5(a), 5(b), 6(c), and 6(d). All are for aiding flow situation (case I) for two RI values of 0.1 and 2.0 and for two Reynolds numbers, 50 and 200. Here, $RI = 0.1$ and 2.0 indicate two different regimes of flow; the first one is a forced convection dominated flow problem and the second case signifies a natural convection dominated situation. There is a hot fluid flow entering from the top of the annulus, passing through a channel between the cold inner cylinder surface and the insulated outer cylinder surface, and is coming out at the exit of the outer cylinder. The isotherms for a Reynolds number of 50 in Figs. 5(a) and 5(b) and for two Richardson numbers of 0.1 and 2.0 show large temperature gradients on the upper part of the inner cylinder and the fluid is cooled all along the inner cylinder wall. Clearly, the heat transfer along the inner cylinder wall is mostly carried out by the forced and natural convection. In both cases, thin hydrodynamic and thermal boundary layers are observed near the cold inner cylinder wall. A comparison of the temperature contours of the above figures shows that in the forced convection dominated situation ($RI = 0.1$) the fluid that comes out from the exit is much colder than that of the case when natural convection effect is dominating ($RI = 2.0$). For $Re_D = 50$, there is a small individual convection cell visible in the upper part of the annulus near the outer cylinder, but there is no reverse flow near the bottom part of the annulus for $RI = 2.0$. Hence, the heat from the surface is mostly transferred by natural convection by the fluid entering from the inlet and passing through the annulus. The recirculation flow results from natural convection combined with boundary conditions specified at the exit.

As Reynolds number increases, Figs. 6(c) and 6(d) show that the thermal boundary layer around the upper part of the inner cylinder wall has become very thin as expected, i.e., after about 60° and beyond (refer to 6(c)) and after about 25° and above (refer to 6(d)). For $Re_D = 200$, the streamlines show the formation of a reverse flow and a large separate convection cell near the outer cylinder wall compared to the corresponding previous cases for $Re_D = 50$. In general, the flow field is characterized by a primary clockwise recirculation bubble near the outer cylinder wall where the shear driven flow by the fluid is impacted on the outer wall and forced to move downward. A large recirculation flow is

observed at higher Reynolds numbers. With the increase of Re_D , the fluid flow from the entrance is increased, the higher velocity fluid passes above the upper part of the cooled surface and gets cooled. As a result, the thermal buoyancy force manifests itself only in the lower part of the domain. The isotherms for higher Re_D show that as Re_D increases, the role of natural convection becomes negligible, and forced convection plays the dominant role in heat transfer. The streamlines and the isotherms for $Re_D = 50$ and 200; and $RI = 0.1$ and 2.0 show clearly that heat transfer is increased by increasing Re_D and RI . The strength of the imposed flow plays an important role on the flow patterns and isotherms through creating the larger sizes of the recirculation bubble near the outer cylinder wall.

From Figs. 5(a, b) and 6(c, d) the developments of the thermal boundary layer growth on the inner cylinder and the effect of flow separation on the temperature contours can be seen. Presented temperature contours reveal that the separation angle is a function of both Reynolds and RI numbers. For a fixed RI number, the separation occurs earlier when the Reynolds number is lower. For a higher Reynolds number a significant change of the separation angle from the inlet is observed when RI number varies but for lower Re_D , there is an insignificant effect on the separation angle for different RI values. For a fixed Reynolds number, the flow separation occurs earlier for smaller values of RI . Due to the difference in the locations of flow separation on the inner cylinder, the extent and strength of the formation of wakes vary which reduce and create different rates of heat flux at the outlet for various Reynolds and RI numbers. Near the outlet, the flow could be unsteady in nature because of the development of the wakes. The present steady state simulation might have not captured correctly the heat and fluid flow phenomena in these regions. For accurate predictions, detail and close examinations of the flow and temperature fields are required in the mixed convection phenomenon.

7.2 Local Nusselt Number Distributions for Case I

The distribution of the local Nusselt number (Nu_i) along the inner cylinder wall (Nu_i is defined by Eqn. [10]) for the same configuration presented in Fig.1 and for four different regimes of flow, viz., purely forced convection ($RI = 0$), dominating forced convection ($RI = 0.1$ and 0.5), mixed convection ($RI = 1.0$), and dominating natural convection ($RI = 2.0$) and for four different Reynolds numbers (Re_D) = 50, 100, 150 and 200 are shown in Figs. 7(e), 7(f), 7(g) and 7(h). The intermittent character of the thermal boundary layer can be observed as the local heat transfer is increased at the top of the inner cylinder. At different Reynolds numbers and to some extent on the upper part of the inner cylinder, the increment of local Nusselt number is almost the same for four different flow regimes. The influence of RI and Re_D can be seen later, particularly towards the bottom part of the inner cylinder. As expected, increasing imposed flow enhances the local heat transfer, which is more pronounced on the upper part of the inner cylinder as seen through Figs. 7(e)-7(f). Heat transfer from the lower part of the inner cylinder is mainly due to forced and natural convection and that through the exit is by natural convection with little contribution from forced convection. At $RI = 0$ (purely forced convection), local heat transfer is at the lowest level for every Re_D compared to the dominating forced convection, mixed convection, and dominating natural convection situations.

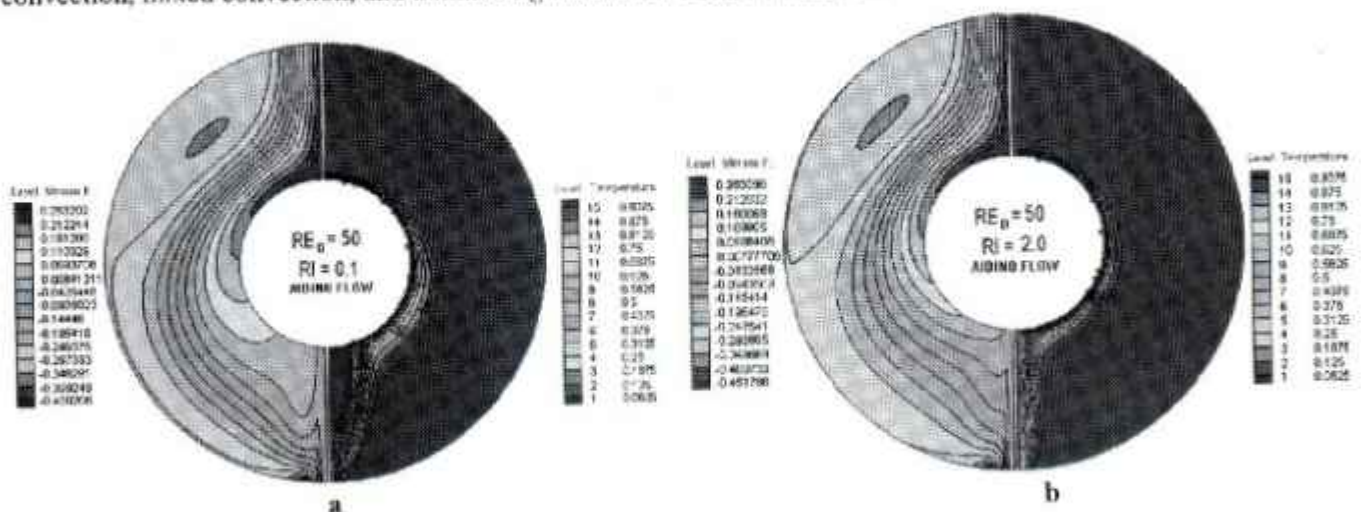


Fig. 5: 2-D views of streamline (dimensionless) and isotherm (dimensionless) contours (a, b) for two different Richardson numbers at Reynolds number (Re_D) of 50 for case I

Mixed Convection in a Ventilated Concentric Horizontal Cylindrical Annulus for Aiding and Opposing Buoyancy Forces

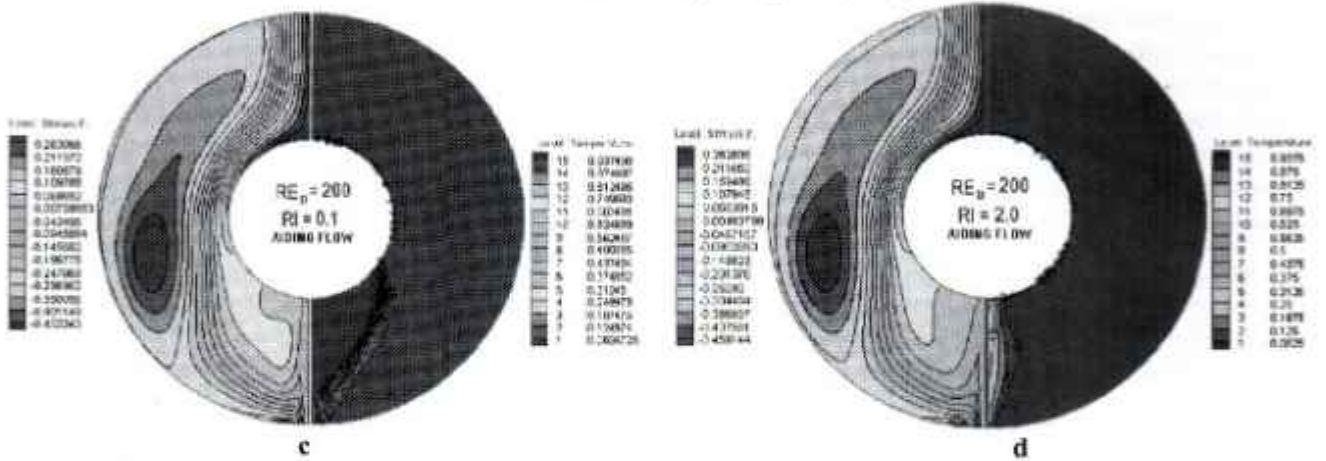


Fig. 6: 2-D views of streamline (dimensionless) and isotherm (dimensionless) contours (a,) for two different Richardson numbers at Reynolds number (Re_D) of 200 for case I

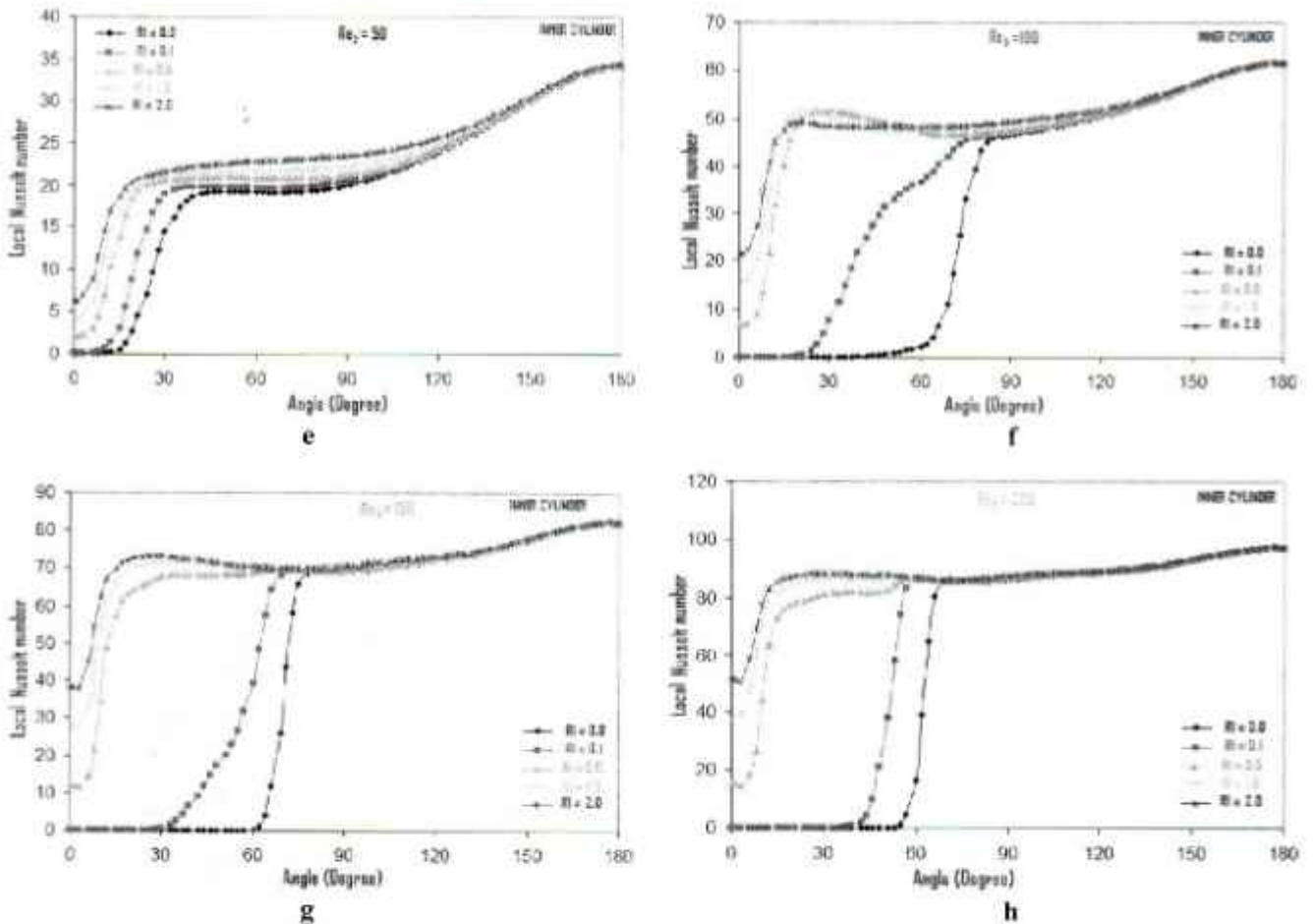


Fig. 7: The local Nusselt number on the inner cylinder wall in case of aiding flow (case I) for various Richardson numbers at Reynolds number (e) 50, (f) 100, (g) 150, and (h) 200

Local heat transfer is almost insignificant at the lower part of the inner cylinder wall for $RI = 0$ and 0.1 and the extent of this region increases with increasing Re_D . From Figs. 5(a) and 6(c), it is observed that at $RI = 0.1$, the fluid is vertically downward in the stagnant zone and conduction and natural convection are the principal modes of heat transfer in that zone. In the dominating forced convection flow regimes i.e., $RI = 0.1$, the local heat transfer rate at the lower symmetry plane is negligible due to the separation of the flow and for weak buoyancy effect. In case of mixed and dominating natural convection flow regimes, the local Nusselt number increases sequentially at the lower

symmetry plane with the increased imposed flow because of increased natural convective effects. It is seen that Nu_L is an increasing function of θ (θ is equal to zero at the lower symmetry plane) with increased RI because the buoyancy force is acting in the imposed flow direction in case of aiding flow situation. As a result, the natural convection effect is enhanced with the increase of RI.

7.3 Characteristics of Flow and Thermal Fields for Case II

Here, the results are discussed for an opposing flow situation (case II). In this case, the inner cylinder wall is at a higher temperature compared to the inlet fluid jet entering the annulus from the top. The isotherms and streamlines for Reynolds number 50 and 200, and two Richardson numbers 0.1 and 2.0 are presented in Figs. 8(i), 8(j); and in Figs. 9(k), 9(l), respectively. For $Re_D = 50$ and 200, the streamlines are similar to those of Figs. 5(a), 5(b); and. 6(c), 6(d) except the fact that the fluid is separated from the wall of the inner cylinder much earlier compared to case I. In case II, for the forced convection situation the fluid gets more heated and comes out of the exit. For the natural convection case, the fluid attains lower energy and exits at a lower temperature. The above situation is further enhanced when the Re_D is increased as can be seen in Figs. 9(k, l). In the opposing flow case, the isotherms spread out more than the aiding flow case. This indicates that a lower temperature gradient prevails near the inner cylinder in case of opposing flow than aiding flow situations. For an opposing flow, due to the unfavorable manifestations of the buoyancy effect, heat transfer rate is decreased in comparison to that of an aiding flow for the same parametric conditions.

7.4 Local Nusselt Number Distributions for Case II

The local Nusselt number along the inner cylinder is calculated for various RI and Re in the opposing flow case. Here, the heat exchange occurs between the hot inner cylinder surface and the cold inlet fluid. As the cold fluid descends from the top it gains heat from the heated inner cylinder and it becomes relatively warmer than the inlet temperature. The warm fluid then comes out at a higher temperature through the exit vent. The heat transfer through the upper inner cylinder surface is generally higher for each Re_D and RI since the influence of forced convection is predominant there and this results in the increase of heat transfer from the top of the inner cylinder into the cold fluid. In case of pure and dominating forced, mixed, and natural convection flows regimes, it is seen that for opposing flow, at each Re_D , the local heat transfer rate is generally higher for up to some extent of the upper portion of the inner cylinder wall compared to case I. From Figs. 8(j) and 9(l), it is observed that at $Re_D = 50$ and 200, a strong reverse flow occurs and a big recirculation cell is formed near the inner cylinder in the lower portion of the domain and this cell is not seen to form for aiding flow situation. An anomalous phenomenon occurs for $RI > 0.1$ because the buoyancy force opposes the imposed flow in a nonlinear fashion which can be seen in Figs. 10(m)-10(p).

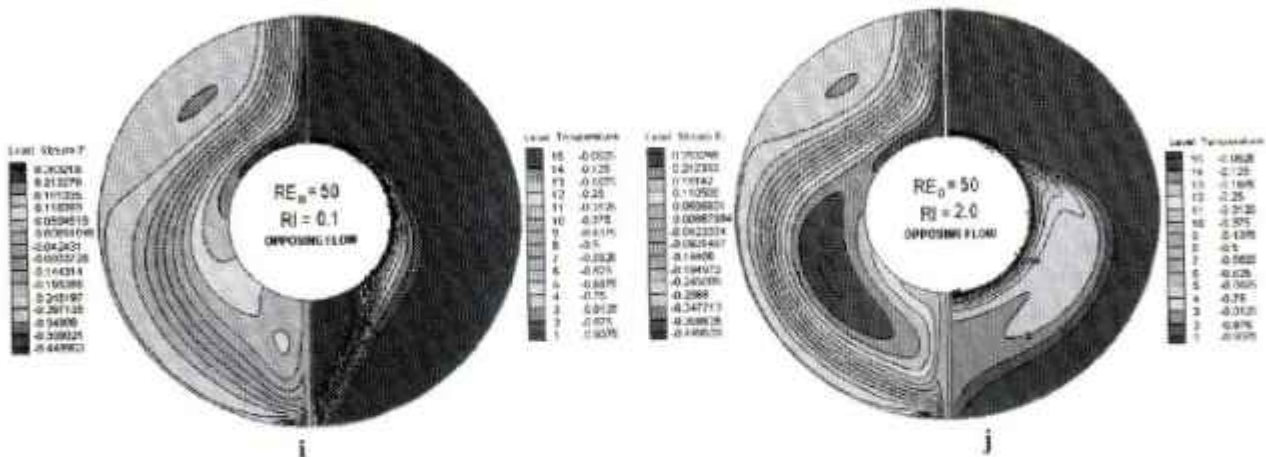


Fig. 8: 2-D views of streamline (dimensionless) and isotherm (dimensionless) contours (i, j) for two different Richardson numbers at Reynolds number (Re_D) of 50 for case II

In opposing flow situation, the thermal buoyancy force opposes the momentum of the incoming jet and helps to separate the flow on the inner cylinder earlier compared with aiding flow situation. As a consequence of this, the wake forms earlier from the top which in turns results in inconsistent behavior in this regime. From Figs. 8(i, j) and 9(k, l), the effects of separation and thermal boundary layer growth on temperature contours can be found. Presented temperature contours reveal that the separation angle is a strong function of Reynolds numbers, but it is almost

Latifa Begum
 Mixed Convection in a Ventilated Concentric Horizontal Cylindrical
 Annulus for Aiding and Opposing Buoyancy Forces

independent of RI numbers. For a fixed RI, the flow separation occurs earlier when the Reynolds number is lower and compared to the aiding flow situation the flow separations occurs faster for a given Re_D and RI numbers.

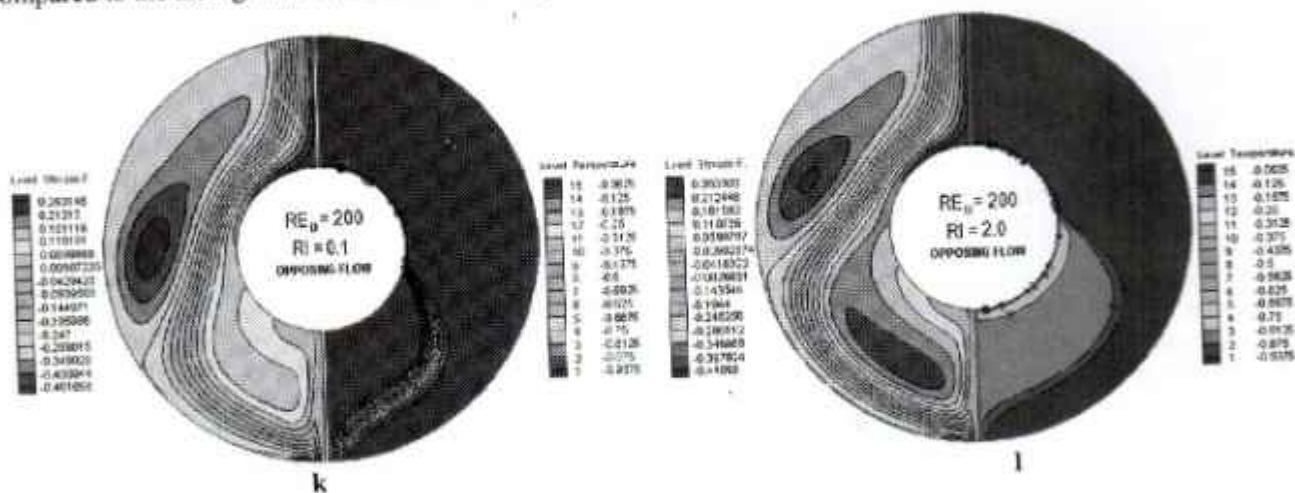


Fig. 9: 2-D views of streamline (dimensionless) and isotherm (dimensionless) contours (k, l) for two different Richardson numbers at Reynolds number (Re_D) of 200 for case II

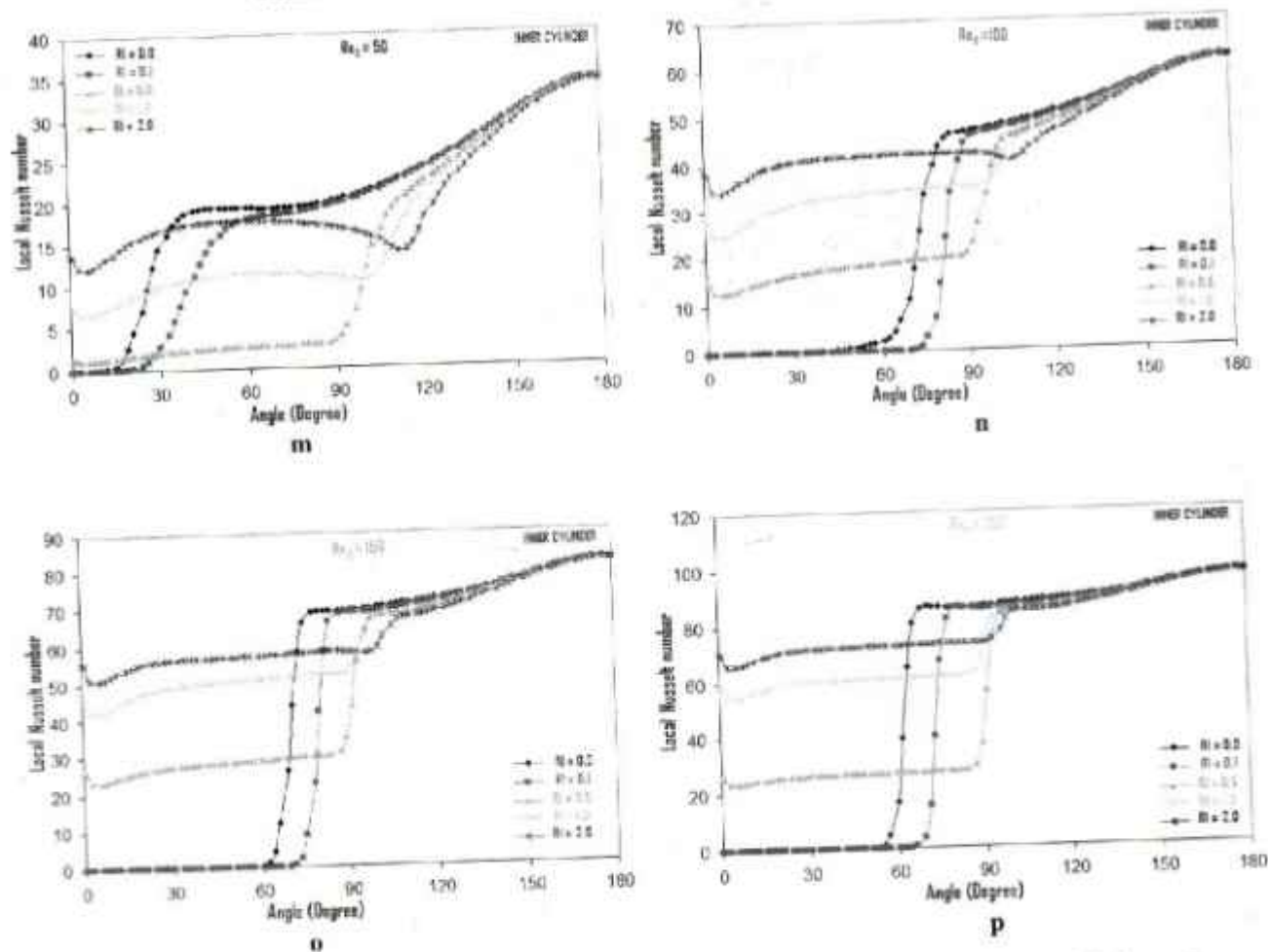


Fig. 10: The local Nusselt number on the inner cylinder wall in case of opposing flow (case II) for various Richardson numbers at Reynolds number (m) 50, (n) 100, (o) 150, and (p) 200

7.5 Average Nusselt Number For Case I And Case II

The effect of the RI on the average Nusselt number is examined for $Re_D = 50, 100, 150,$ and 200 when buoyancy forces near the inner cylinder aids and opposes the inlet forced flow. The predicted average Nusselt number results for mixed aiding flow and mixed opposing flow situations are presented through Figs. 11 and 12. From Fig. 11, it can be seen that Nu_{avg} increases with the increase of Re_D , but for $RI > 1.0$, Nu_{avg} remains practically unchanged. For purely forced convection situation Nu_{avg} is the minimum for all cases. For opposing flows, shown in Fig. 12, Nu_{avg} is higher with the increase of Re_D for all RI. For a fixed Re_D , Nu_{avg} decreases first and then gradually increases with RI. In each case, Nu_{avg} attains almost a constant value at about $RI > 1.5$. At $Re_D = 50$, for opposing flow, the heat transfer rate is maximum when $RI = 0$ (purely forced convection). The increase of the Richardson number leads to an increase the strength of the buoyancy force. Since in this study a very limited range of RI is considered which has not appreciably increased the Grashof number and the corresponding buoyancy force.

A comparative study of aiding and opposing flow cases was performed and is presented in the form of average Nusselt number as a function of Re_D for different RI in Figs. 13, 14, 15 and 16. It can be deduced that the average Nusselt number increases with increasing Re_D . For all RI, the Nu_{avg} is greater for mixed aiding flows compared to mixed opposing flows. These figures also show that for all RI for mixed aiding flow Nu_{avg} is greater in relation to the purely forced convection flow. For $RI = 0.1$, the Nu_{avg} for the opposing flow is always lower than the purely forced convection situation (Fig. 13). For $RI = 0.5$, the Nu_{avg} for the opposing flow for Re_D up to about 80, is lower than purely forced convection flow whereas for $Re_D > 80$ it is higher (Fig. 14). This is due to the fact that the buoyancy force is weaker for $RI = 0.5$. With the increase of Re , the forced flow for this case increases more rapidly. In Fig. 15, it is seen that for $RI = 1.0$, the Nu_{avg} is smaller in value for the opposing flow condition compared to the purely forced convection flow situation up to about $Re_D \leq 60$. For $RI = 2.0$, Nu_{avg} is greater for opposing flow condition after $Re_D = 50$ than the value obtained for $RI = 0$ (Fig.16).

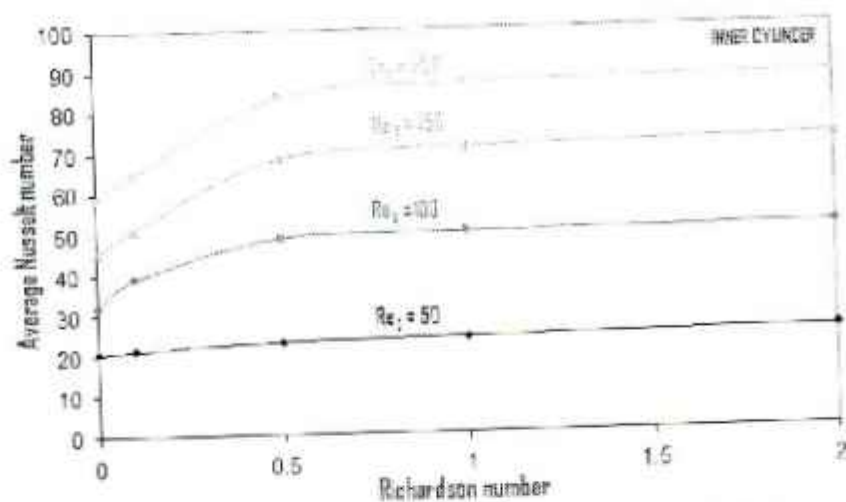


Fig. 11: Variation of average Nusselt number on the inner cylinder wall with Richardson numbers for various Reynolds number of 50, 100, 150, and 200 during the aiding flow situation (case I)

Mixed Convection in a Ventilated Concentric Horizontal Cylindrical Annulus for Aiding and Opposing Buoyancy Forces

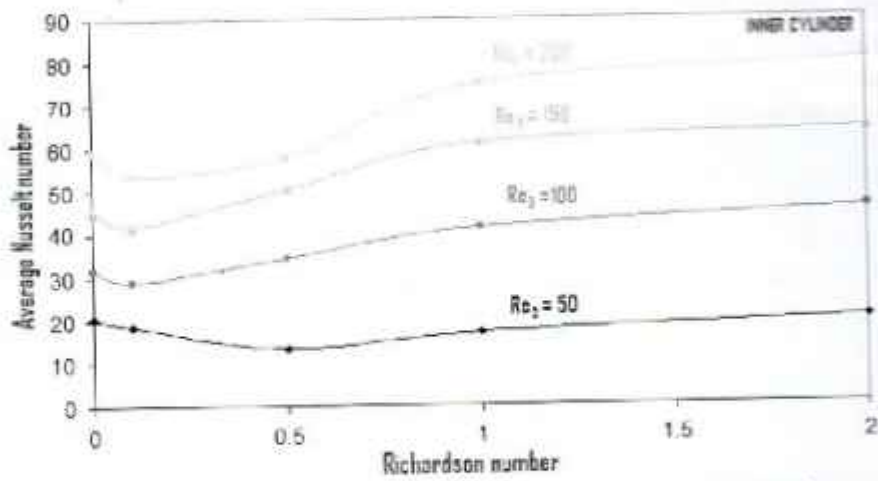


Fig. 12: Variation of average Nusselt number on the inner cylinder wall with Richardson numbers for various Reynolds number of 50, 100, 150, and 200 during the opposing flow situation (case II)

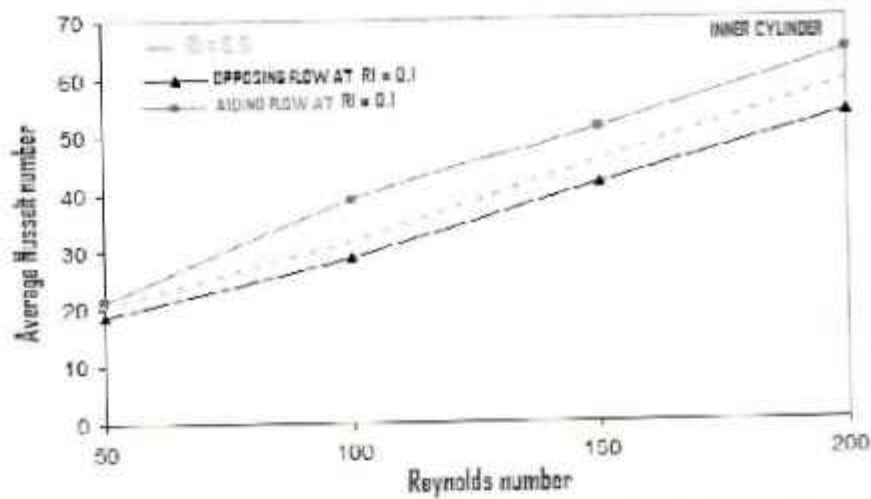


Fig. 13: Variation of average Nusselt number on the inner cylinder wall with Reynolds numbers at Richardson number of 0.1 during the aiding (case I) and opposing (case II) flow situations

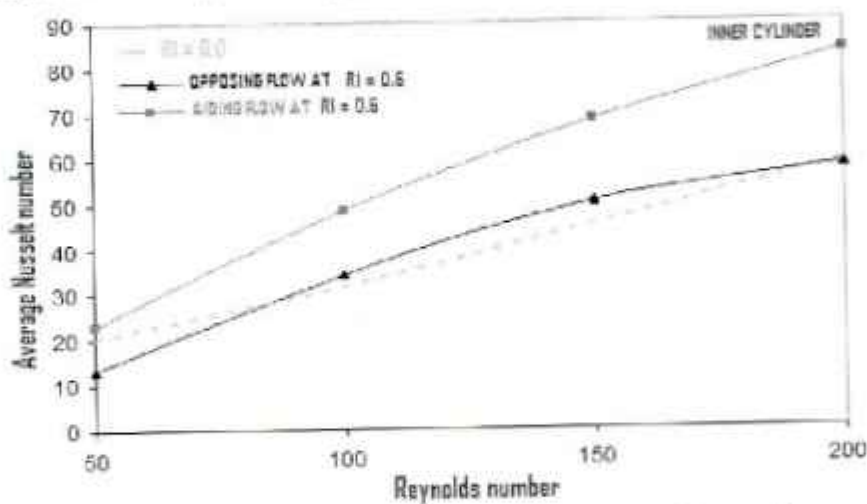


Fig. 14: Variation of average Nusselt number on the inner cylinder wall with Reynolds numbers at Richardson number of 0.5 during the aiding (case I) and opposing (case II) flow situations

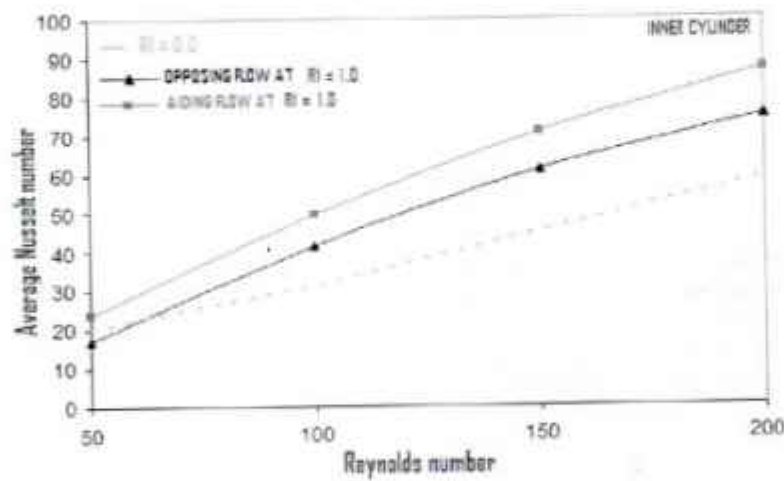


Fig. 15: Variation of average Nusselt number on the inner cylinder wall with Reynolds numbers at Richardson number of 1.0 during the aiding (case I) and opposing (case II) flow situations

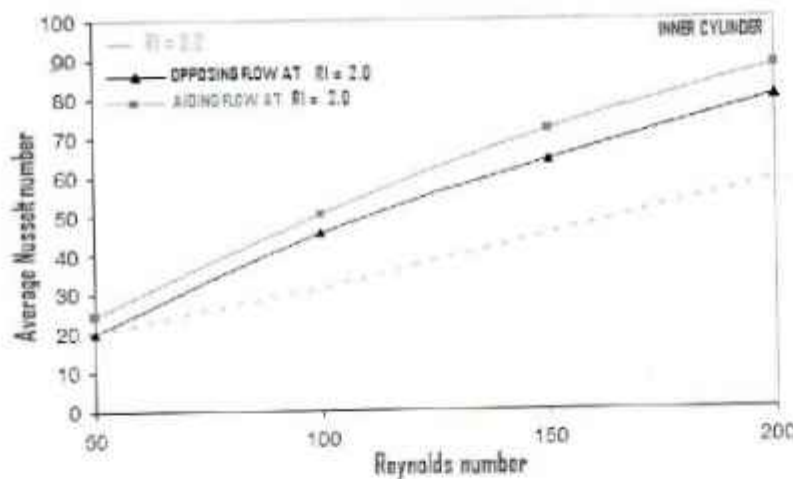


Fig. 16: Variation of average Nusselt number on the inner cylinder wall with Reynolds numbers at Richardson number of 2.0 during the aiding (case I) and opposing (case II) flow situations

The Nu_{avg} values for water in mixed aiding flow situation are correlated using the multi-linear least-squares regression analysis and can be represented by:

$$Nu_{avg} = 0.7315 (RI)^{0.091} (Re_D)^{0.903}, \quad 0.1 \leq RI \leq 2.0, \quad 50 \leq Re_D \leq 200, \quad R^2 = 98.5\% \quad (13)$$

For the opposing flow situation, the correlation of Nu_{avg} is represented by:

$$Nu_{avg} = 0.4059 (RI)^{0.116} (Re_D)^{0.982}, \quad 0.1 \leq RI \leq 2.0, \quad 50 \leq Re_D \leq 200, \quad R^2 = 95.4\% \quad (14)$$

The overall correlation coefficient for aiding and for opposing flow situations shows that the fit of the data is excellent in the range of the parameters considered in this study. From the above correlations, it is observed that under identical geometric and thermal conditions, the mixed aiding flow leads to a higher heat transfer rate than the mixed opposing flow situation as can be seen from the higher constant multiplying factor. It is further seen that for opposing flow, the average Nusselt number is slightly more sensitive with regard to Richardson number and Reynolds number compared to the adding flow situation.

8.0 CONCLUSIONS

A numerical study has been carried out on mixed convection heat transfer (laminar natural convection and forced convection) in the annulus between two horizontal concentric cylinders for aiding and opposing buoyancy driven flows. It is found that the average Nusselt number is affected considerably by the imposed flow, and the strength of

the buoyancy force. Markedly different flow behaviors are observed between the above two different flow situations. For the aiding flow case, the average Nusselt number increases monotonically with the increase of the Richardson number up to the value of about 1.0 and then it remains practically unchanged beyond that value and this is true for all Re_D studied in this investigation. In case of opposing flow, it first decreases and then it increases with the increase of RI up to a value of about 1.5, after that it remains almost constant for all the values of the studied Re_D . The average Nusselt number is an increasing function of the imposed flow rate for both situations. For the aiding flow, since the imposed flow is stratified (top heated fluid above the cold fluid in the annulus), some flow stratification at the bottom regions is also observed for all different studied cases. The local Nusselt number at the upper part of the inner cylinder has a high value and it decreases very slowly to some extent along the inner cylinder and this trend is independent of the flow regime. After the slow decrease, the local Nusselt number then decreases rapidly to a small value at the lower part of the inner cylinder for both aiding and opposing flow conditions. At the lower part of the inner cylinder, heat transfer rate is insignificant for $RI \leq 0.1$, because of the weak buoyancy force effect for both cases. The local Nusselt number near the bottom part of the inner cylinder exhibits an oscillatory behavior for various Re_D and RI numbers. This oscillatory behavior is due to various effects, namely, wake formation, the location of the separation of the flow, the developments of thermal boundary-layer and the presence of weak natural convection. Based on the flow visualization, computations predict earlier separation of the flow in case of opposing flow compared to the aiding flow. This is due to the opposing effects of the thermal buoyancy force on the inlet jet. For a better explanation of the results, the location of the separation point and the formation of the wake region require a more careful examination of the flow and thermal fields near the surface of the inner cylinder. For the limited range of parameters studied in this investigation, it is observed that the average Nusselt number is significantly higher for mixed aiding flow than mixed opposing flow. Correlations for the average Nusselt number (Nu_{avg}) against RI and Re_D are developed to evaluate the effect of RI and Re_D on Nu_{avg} for both the aiding and opposing flow situations. These correlations will help in designing vented horizontal tubular heat exchangers.

ACKNOWLEDGMENTS

This work is partially supported by the National Sciences and Engineering Research Council (NSERC) of Canada Discovery Grant RGPIN48158 awarded to M. Hasan of McGill University, Montreal, for which authors are grateful.

REFERENCES

- [1] Hussein, A. K., 2013, "Mixed Convection in Cylinders - A Comprehensive Overview and Understanding," *J. Basic. Appl. Sci. Res.*, 3(10), ISSN 2090-4304, pp. 328-338.
- [2] El-Maghlany, W. M., Teamah M. A., Sorour, M. M., and Aziz, H. M. A., 2014, "Numerical Simulation of Double Diffusive Laminar Mixed Convection in a Horizontal Rotating Annulus: Part (I): Effect of Richardson and Lewis numbers," *CFD Letters*, 6 (1), pp. 32-46.
- [3] Jafari, S., Jafari, S., and Rahnama, M., 2018, "Simulation of Mixed Convection in Eccentric Annulus: A Combined Lattice Boltzmann and Smoothed Profile Approach," *Heat Transfer Engineering*, 38(1), pp. 1-15.
- [4] Kuehn, T. H., and Goldstein, R. J., 1976, "An Experimental and Theoretical Study of Natural Convection in the Annulus Between Horizontal Concentric Cylinders," *J. Fluid Mech*, 74, pp.695-719.
- [5] Patankar, S. V., 1980, "Numerical Heat Transfer and Fluid Flow", Taylor & Francis, London.
- [6] Hessami M. A., Pollard, A., and Rowe R. D., 1984, "Numerical Calculation of Natural Convective Heat Transfer Between Horizontal Concentric Isothermal Cylinders-Effects of the Variation of the Fluid Properties," *J. Heat Transfer*, 106, pp.668-671.
- [7] Yang, H. Q., Yang, K. T., and Lloyd, J. R., 1988, "Natural Convection Suppression in Horizontal Annuli by Azimuthal Baffles," *Int. J. Heat Mass Transfer*, 10, pp.2123-2135.
- [8] Marie-Isabelle, F., André, G., and Saint-Louis, K., 1997, "Study of Heat Transfer in a Horizontal Cylinder With Fins," *Rev Gén Therm*, 36, pp.398-410.
- [9] Begum, L., 2008, "Natural and Mixed Convection in a Horizontal Cylindrical Annulus with and without Fins on Inner Cylinder," M.Eng. Thesis, Department of Mining and Materials Engineering, McGill University, Canada.